Prepared for submission to JINST

European Conference on Plasma Diagnostic, 7^{th} - 11^{th} June 2021, Salamanca, Spain

Design and first measurements of the divertor Thomson scattering system on the ASDEX Upgrade tokamak

B. Kurzan,[1] **A. Lohs, G. Sellmair, M. Sochor, and ASDEX Upgrade team**[2]

Max Planck Institute for Plasma Physics, Boltzmannstr. 2, 85748 Garching, Germany

E-mail: Bernd.Kurzan@ipp.mpg.de

Abstract: A new divertor Thomson scattering system was installed on the ASDEX Upgrade tokamak, to measure profiles of electron density and temperature in the lower divertor along a poloidal cord, starting in the outer divertor, crossing the x-point, and ending on the high field side. No direct access to these regions from outside the vacuum vessel is possible. So critical parts of the laser beam line, and the light collection system had to be installed inside the vacuum vessel. Details of the design and first measurements are presented in this article.

Keywords: Thomson scattering, magnetic divertor, magnetic confinement

[1]Corresponding author.

[2]See author list of H. Meyer et al., *Nucl. Fusion* **59** (2019) 112014.

Contents

1 Introduction

On several magnetic fusion devices magnetic divertors are used for controlling the impurity content of the main chamber plasma. For the measurement of electron density and temperature with high spatial resolution in the divertor, Thomson scattering (TS) systems are, and will be used. Divertor TS systems exist on DIIID [1] [2] [3], and TCV [4]. They are being designed on MAST Upgrade [5], NSTX-U [6], JT-60SA [7], and ITER [8].

Divertor physics is also a main field of interest at the ASDEX (Axial Symmetric Divertor Experiment) Upgrade tokamak. On ASDEX Upgrade (AUG) divertor TS (DTS) therefore was foreseen from the beginning [9], but was not realized in the planned geometry: the simple approach of employing the lasers used for core TS also for DTS became impossible after changing the open divertor geometry used in the early years of AUG to the LYRA configuration [10], where since then these lasers run behind the divertor plates, where no plasma of interest exists.

A new DTS system with a separate laser was installed with scattering volumes along a poloidal cord, which starts at the outer divertor plate, runs through the x-point and ends on the high field side. With such a TS system local quantitative information about the electron density and temperature in the divertor volume can be obtained, which is not possible with other methods like e. g. Langmuir probes, or spectroscopy.

The paper is organized as follows: The specifications, the design, and the calibration of the DTS system are introduced in section 2. Examples of measured profiles are presented in section 3.

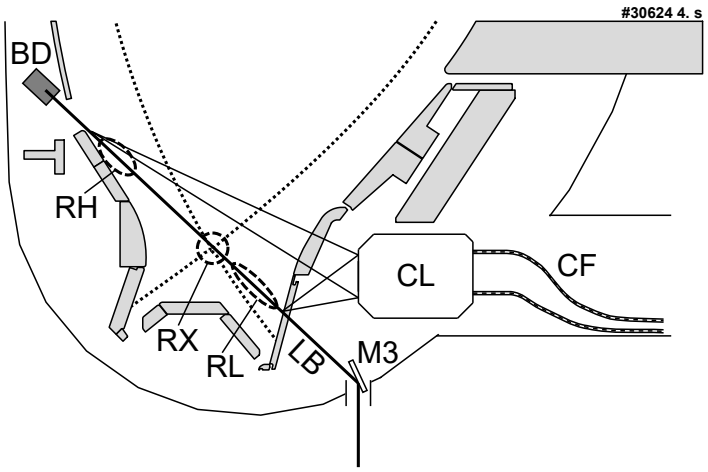

Figure 1. Poloidal cross section of the scattering geometry. The laser beam (LB) runs over a mirror (M3) to the three ROIs (RL, RX, RH) for a dedicated magnetic reference equilibrium (#30624, t= 4.0 s), and finally to the beam dump (BD). The scattered light is coupled to optical fibers (CF) by the collection lens (CL).

2 Specifications, design, calibration and commissioning of the DTS system

The design of the DTS system is determined by the regions of interest (ROIs) in the lower divertor chamber, the access possibilities by the laser beam line and the observation optics. The Thomson scattered light is analyzed with polychromators which are designed to meet the expected range of electron densities and temperatures.

2.1 Specifications

The ROIs in the lower divertor, which shall be covered by the DTS system, are the regions above and along the outer divertor leg, the x-point, and the region of the high density front in the far scrape-off layer on the high field side [11] (see the ROIs marked by RL, RX, and RH in figure 1). Access to these regions defines the laser beam path (LB in figure 1) inside the vacuum vessel. Both a laser mirror (M3), the laser beam dump (BD), and the collection lens (CL), which couples the Thomson scattered light to fiber guides (CF), must be installed inside the vacuum vessel (see figure 1), which complicated the realisation of DTS.

2.2 Laser beam line

The laser beam line, the light collection and detection optics are shown schematically in figure 2: The beam of the laser (L) is guided via 3 mirrors (M1, M2, M3) to the scattering volumes in the plasma, and is finally absorbed by the beam dump (BD). The mirrors M1 and M2 are tiltable, to align the laser beam to mirror M3 (not tiltable) and the beam dump BD. At the transition from air to vacuum the laser beam passes two Brewster windows (B1, B2). This is for safety reasons: In the case of damaging one Brewster window by the laser, loss of vacuum is avoided.

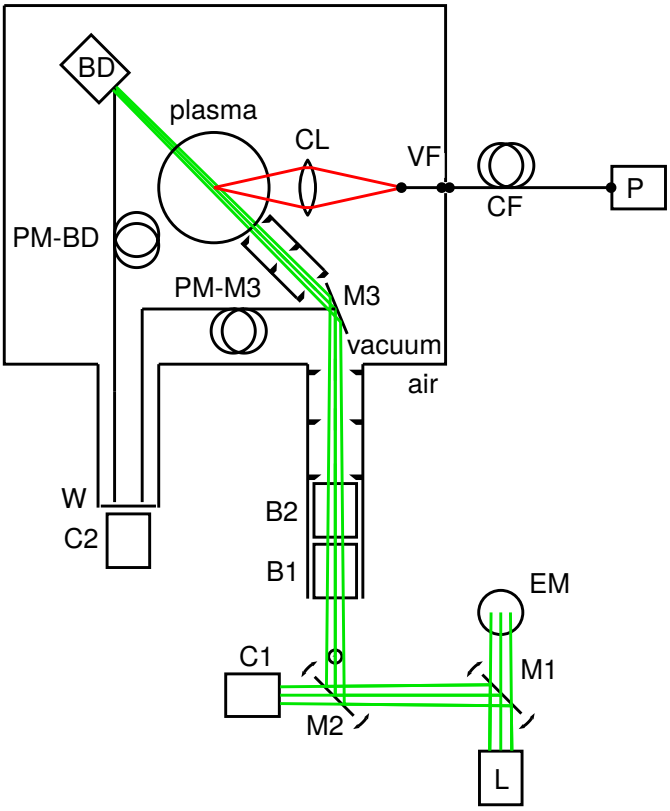

Figure 2. Schematic of the laser beam line and light collection path. The laser beam line consists of laser (L), energy monitor (EM), mirrors (M1, M2, M3), two Brewster windows (B1, B2) and beam dump (BD). The laser beam profile is checked with camera C1. The laser beam positions at mirror M3 and at the beam dump are monitored via optical fiber guides (PM-M3, PM-BD) through a vacuum window (W) by camera C2. The signal path consists of the collection lens (CL), optical fiber guides (CF), the vacuum feed-throughs (VF) and the polychromators (P).

The beam dump, located in vacuum, consists of absorbing glass plates. The laser beam enters the glass under Brewster angle, to minimize back reflections. The heat capacity of the passively cooled beam dump is limited: It was tested in the laboratory that it stands laser operation with pulse energy 700 mJ, and repetition rate 20 Hz for the duration of an ASDEX Upgrade plasma discharge, which is up to 10 s long.

The laser beam profile is checked with camera C1. The positions of the laser beam on the mirror M3 and the beam dump are monitored by 4 fiber guides each (PM-M3, PM-BD) via a camera (C2) through a vacuum window (W). The fibers have a diameter of 480 μm and are located behind the absorbing glass of the beam dump, and behind the mirror M3 respectively. The shine through of the laser beam lights the fibers. They are arranged such that all 4 fibers each are illumiated by the outer edge of the laser beam profile, if the laser beam is in its correct position. The fiber core is made out of pure silica, so a degradation of the transmission due to neutron irradiation is expected not before 5 to 10 years.

The energy of the laser is measured by the energy monitor (EM). It consists of an integrating

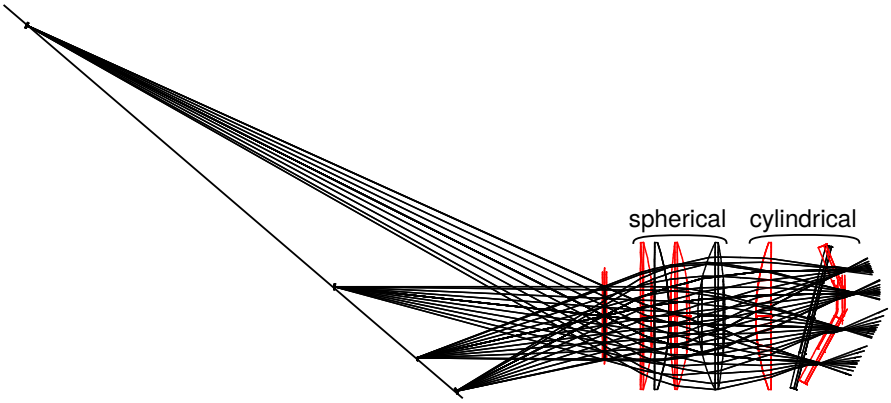

Figure 3. Optical design of the collection lens.

sphere and a fast PIN photodiode. The collection lens (CL) couples the scattered light into optical fibers (CF) guiding the light via vacuum feed-throughs (VF) to the polychromators (P).

For Thomson scattering a pulsed Nd-YAG laser with wavelength 1064 nm, and repetition rate 20 Hz is used. The laser has, due to its built-in telescope optics, a converging beam with a diameter of 8 mm at the position of the scattering volumes, which are at a distance of around 5.5 m away from the laser. The dielectric mirror M3 is located in vacuum. It has a special hard coating (HR type 2 manufactured by Laseroptik, Garbsen, Germany), deposited by ion beam sputtering, and thus has the same high laser induced damage threshold both in air, and in vacuum. Inspection of the in-vessel components of the diagnostic after two experimental campaigns showed, that mirror M3 of the laser beam line had changed its orientation and that the laser beam was hitting a baffle and was back reflected on mirror M3. To avoid this in the future the identified mechanical structures were reinforced. If mirror M3 inside the vacuum vessel would be damaged again by the laser beam, it is impossible to replace it during an experimental campaign, because the vacuum vessel is closed over several months. Two measures were taken to reduce this risk: a) An injection-seeded laser is used now, which emits a continuous pulse without high intensity spikes, which can damage dielectric mirrors [12]. b) The laser is operated at a pulse energy of only 400 mJ, to limit the energy deposited in the beam dump and on the mirror M3. It was found that this pulse energy is enough for obtaining good scattering signals.

Laser light can potentially illuminate parts of the ASDEX Upgrade inner wall, which are viewed by the collection lens, and thus can lead to high laser stray light levels. This is reduced by encapsulating the laser beam on its way to the divertor chamber in fully baffled and light tight pipes.

2.3 Light collection path

For the collection lens the scattering volumes are located within an angle of view of around 45^o. The optical design of the collection lens is shown in figure 3. Due to space restrictions the fiber guides on the image side of the collection lens must be parallel to the horizontal pump port of the vacuum vessel. This parallelisation of the optical path is achieved with an image-side telecentric design. The laser beam is tilted by 40^o with respect to the optical axis of the collection cell. The collection lens is therefore also anamorphic, to image an area around the scattering volume of about

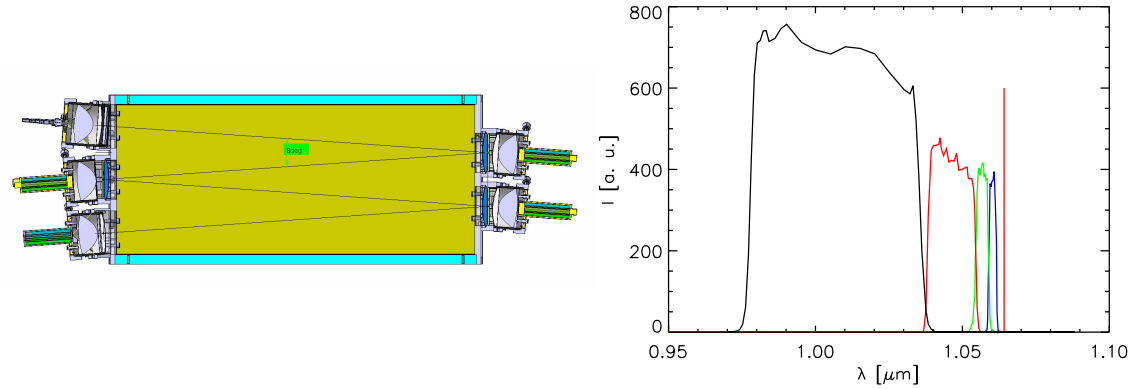

Figure 4. Optical design of a polychromator and typical relative sensitivities of the spectral channels.

1 cm length along, and of 1 cm width perpendicular to the laser beam onto circular fibers. To maximize the light collection power in this tight geometry a f/0.6 collection lens (according to the definition for circular lenses) is used. It is located behind the divertor tiles. For collecting the scattered light a rectangular aperture between the divertor tiles with a width of 2 cm in the toroidal direction could be realized without compromising divertor performance. So the actual shape of the collection lens is not circular, but rectangular, as given by the aperture between the divertor tiles.

In the image plain of the collection lens the TS light is focused into fibers. Each fiber is routed via individual vacuum feed-throughs out of the ASDEX Upgrade vessel to the polychromators, which are located outside the torus hall. Since the amount of work to produce these vacuum feed-throughs is high, the number of fibers was minimized. So for each spatial channel a single fiber it used. As suitable to the optical requirements, a fiber with diameter 1000 μm and ultra high numerical aperture NA= 0.66 is used. Since the collection lens is inside the vacuum vessel, the fiber must also be compatible with ultra-high vacuum conditions. Such a fiber is of the silica core, Teflon cladding, silicone buffer type. For high transmission in the near infrared the low-OH silica core version was chosen. As a start a number of 24 fibers and thus spatial channels was realized.

2.4 Polychromators

For each spatial channel a separate polychromator is used. The TS spectra expected for the specified electron temperature range of 1 - 100 eV are analyzed with 4 spectral channels. The optical design is of the standard type (see figure 4): the diverging light bundle emerging from the small diameter input fiber is transformed to a low divergence large diameter beam, which passes over the spectral channels successively. Interference filters are used to select the spectral ranges and to suppress the laser stray light in each spectral channel. The suppression for the laser wavelength is > OD6. Typical relative spectral sensitivities of the spectral channels of a polychromator are shown in figure 4. During the commissioning phase in around half of the polychromators some laser stray light was detected in the spectral channel, which is close to the wavelength of the laser. For these spectral channels the filters had to be doubled. The light, which is not transmitted by a filter is reflected to the subsequent filter. The TS light pulses are detected by avalanche photodiodes.

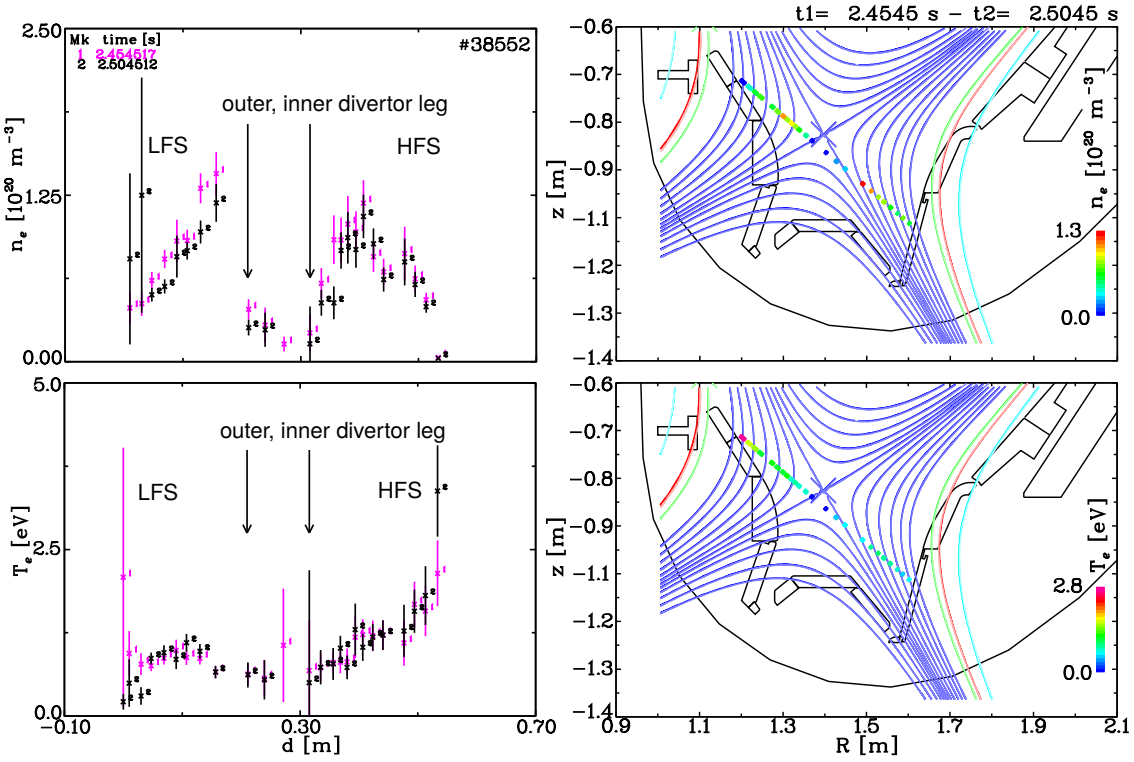

Figure 5. On the left side profiles of electron density n_e and temperature T_e versus the laser beam coordinate d are shown for two neighboring time points for an L mode plasma. The positions of the outer and inner divertor leg are indicated. On the right side the mean values of electron density n_e and temperature T_e over two time points t_1, t_2 are plotted at the positions of the scattering volumes together with the shape of the magnetic equilibrium.

2.5 Data acquisition

The signals of the detectors are sampled by newly developed data acquisition modules (1 GSamples/s, 14 bit resolution), which are tailored to fit for the in-house data link standard SIO2 [13]. With this high bit resolution, both small, and large signals can be recorded with the same amplifier settings for the detectors and sensitvity settings for the data acquisition modules. This has two advantages: (a) Systematic errors between Thomson scattering and calibration data are reduced. (b) For plasmas with low electron densities, or with electron temperatures outside the specified range, the signal amplitudes in the spectral channels decrease and may become comparable to the noise level. When the noise level is resolved with some bits, such small signals can still be detected by employing data processing techniques [14].

2.6 Calibrations

For determining the electron temperature from the relative signal amplitudes of the spectral channels a relative calibration is performed. An absolute calibration is necessary to obtain the electron density. The relative calibration, which is done with an optical parametric oscillator, and the absolute calibration by Raman scattering in nitrogen are analog to the methods described in [15].

3 Examples of measured electron density and temperature profiles

In the following some examples are shown, which demonstrate the actual measurement capabilities of the DTS system.

3.1 L mode

The L mode discharge with shot number #38552 (line averaged density $\overline{n}_e = 4.4 \times 10^{19}$ m^{-3}, toroidal magnetic field B_t = -2.5 T, plasma current I_p = 600 kA, electron cyclotron resonance heating P_{ECRH} = 0.4 MW) is chosen, because here the capability to measure small temperatures is demonstrated. Profiles of electron density n_e and temperature T_e versus the coordinate d along the laser beam are shown in figure 5. The laser beam enters the divertor chamber on the low field side (LFS) at d≈ 0.0 m. In figure 5 also the profiles of electron density and temperature averaged over two time points are plotted in a poloidal plane at the positions of the scattering volumes together with the shape of the magnetic equilibrium. Towards the outer divertor leg the electron density is rising. In the private flux region between outer and inner divertor leg the electron density is low, but not zero. On the high field side (HFS) a high electron density is measured. The electron temperatures are around 0.3 - 2 eV.

Table 1. Electron densities n_e, temperatures T_e, and pressures $n_e \times T_e$ in the midplane, and in the divertor, at the LFS for shot #38552, at the time t≈ 2.5 s.

Position (LFS)	n_e [10^{19} m^{-3}]	T_e [eV]	$n_e \times T_e$ [10^{19} m^{-3} eV]
midplane	0.5	25	12.5
divertor	10	1	10

It is now checked, if the electron pressure is conserved along an open magnetic flux surface connecting the divertor and the midplane of the plasma on the LFS. The electron pressures measured with DTS in the divertor, and with edge Thomson scattering in the midplane of the plasma agree (see table 1).

3.2 H mode

The H mode discharge with shot number #38659 (line averaged density $\overline{n}_e = 4.2 \times 10^{19}$ m^{-3}, reversed toroidal magnetic field B_t = 2.4 T, and plasma current I_p = -810 kA, electron resonance heating P_{ECRH} = 1.5 MW, neutral beam injection heating P_{NBI} = 7.7 MW) is shown in figure 6. Here electron temperatures of up to 200 eV are measuered with DTS, due to the scattering volume being above the x-point in the confined region. This temperature is larger than the designed range of the spectrometers, but it is still possible to measure it, although with increased error bars.

3.3 Standard H mode with Edge Localized Modes

For constant plasma parameters ($\overline{n}_e = 8.1 \times 10^{19}$ m^{-3}, B_t = -2.5 T, I_p = 1.0 MA, P_{ECRH} = 2.7 MW, P_{NBI} = 5.1 MW) in a standard H mode discharge electron density and temperature profiles for different phases of edge localized modes (ELMs) and inter-ELM fluctuations, which are observed with DTS are shown in figure 7. The ELMs deposit heat and particles on the divertor plates, giving rise to poloidal thermo currents [16] measured in the signal Ipolsola. In figure 7 the time points

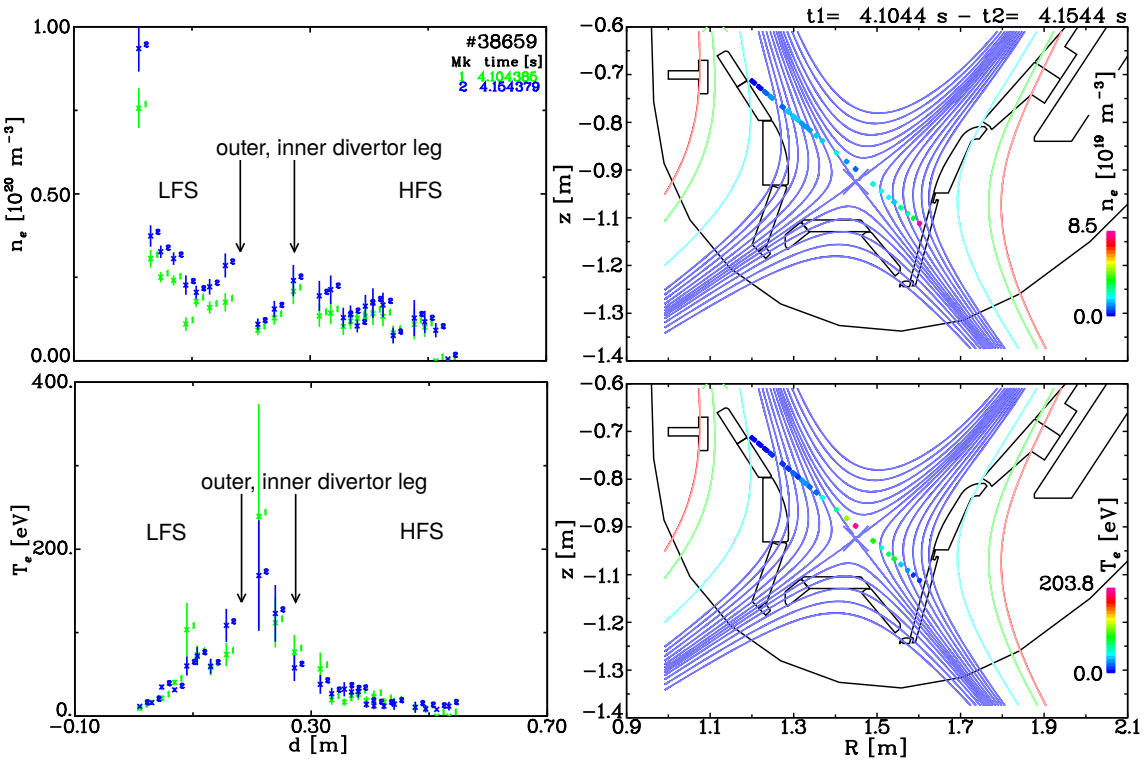

Figure 6. Measured electron density n_e and temperature T_e profiles along the laser beam coordinate d for two neighboring time points for a H mode plasma in reversed I_p, B_t. The positions of the outer and inner divertor leg are indicated. The mean values of electron density n_e and temperature T_e over two time points t_1, t_2 are plotted at the position of the scattering volumes together with the shape of the magnetic equilibrium for a quiescent H mode plasma in reversed I_p, B_t.

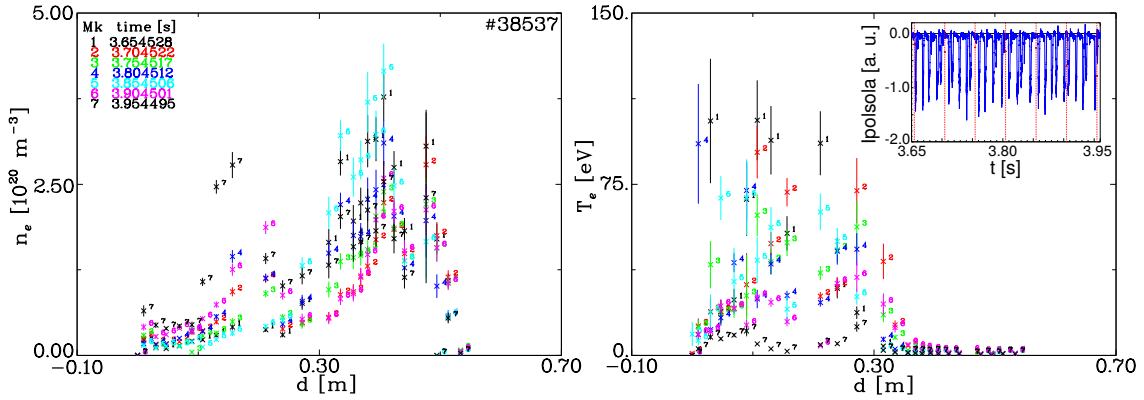

Figure 7. Electron density n_e and temperature T_e profiles along the laser beam coordinate d for a standard H mode plasma during a phase with ELMs. The time points of the DTS profiles are indicated by vertical lines in the insert plot with respect to the thermo current Ipolsola in the outer divertor versus time t.

when the DTS laser was fired are indicated with respect to the thermo currents Ipolsola. As a first interpretation one finds, that during and in-between ELMs, phases of high electron density and low electron temperature and vice versa are measured on the LFS (time points 1 and 7 in figure 7). On the HFS a high electron density and low electron temperature plasma exists. Higher electron densities on the HFS are often correlated with lower electron densities in the outer divertor and vice versa (time points 5 and 6 in figure 7). More detailed interpretations will be the subject of forthcoming work.

4 Conclusion

With the new DTS system electron density and temperature values can now be measured in the lower divertor of AUG. A multitude of divertor plasmas will be characterized with DTS to understand the underlying physics.

Acknowledgments

This work has been carried out within the framework of the EUROfusion Consortium and has received funding from the Euratom research and training program 2014-2018 and 2019-2020 under grant agreement No 633053. The views and opinions expressed herein do not necessarily reflect those of the European Commission.

The reported results would not have been possible without support by M. Huber, L. Kammerloher, K. Kaunert, and W. Zeidner.

References

[1] T. N. Carlstrom, J. H. Foote, D. G. Nilson, and B. W. Rice, *Design of the divertor Thomson scattering system on DIII-D*, *Rev. Sci. Instrum.* **66** (1995) 493

[2] T. N. Carlstrom, C. L. Hsieh, R. Stockdale, D. G. Nilson, and D. N. Hill, *Initial operation of the divertor Thomson diagnostic on DIII-D*, *Rev. Sci. Instrum.* **68** (1997) 1195

[3] F. Glass, T. N. Carlstrom, D. Du, A. G. McLean, D. A. Taussig, and R. L. Boivin, *Upgraded divertor Thomson scattering diagnostic on DIII-D*, *Rev. Sci. Instrum.* **87** (2016) 11E508

[4] P. Blanchard, Y. Andrebe, H. Arnichand, R. Agnello, S. Antonioni, S. Couturier, J. Decker, T. De Kerchove D'Exaerde, B. P. Duval, I. Furno, P.-F. Isoz, P. Lavanchy, X. Liobet, P. Marlétaz, J. Masur, and the TCV team, *Thomson scattering measurements in the divertor region of the TCV tokamak plasma*, *J. Instrum.* **14** (2019) C10038

[5] J. Hawke, R. Scannell, J. Harrison, R. Huxford, and P. Bohm, *Outline of optical design and viewing geometry for divertor Thomson scattering on MAST upgrade*, *J. Instrum.* **8** (2013) C11010

[6] A. G. McLean, V. A. Soukhanovskii, S. L. Allen, T. N. Carlstrom, P. B. LeBlanc. M. Ono, and B. C. Stratton, *Conceptual design of a divertor Thomson scattering diagnostic on NSTX-U*, *Rev. Sci. Instrum.* **85** (2014) 11E825

[7] S. Kajita, T. Hatae, H. Tojo, A. Enokuchi, T. Hamano, K. Shimizu, and H. Kawashima, *Performance of JT-60SA divertor Thomson scattering diagnostics*, *Rev. Sci. Instrum.* **86** (2015) 083511

[8] E. E. Mukhin, G. S. Kurskiev, A. V. Gorbunov, D. S. Samsonov, S. Yu. Tolstyakov, A. G. Razdobarin, N. A. Babinov, A. N. Bazhenov, I. M. Bukreev, A. M. Dmitriev, D. I. Elets, A. N. Koval, A. E. Litvinov, S. V. Masyukevich, V. A. Senitchenkov, V. A. Solovei, I. B. Tereschenko, L. A. Varshavchik, A. S. Kukushkin, I. A. Khodunov, M. G. Levashova, V. S. Lisitsa, K. Yu. Vukolov, E. B. Berik, P. V. Chernakov, Al. P. Chernakov, An. P. Chernakov, P. A. Zatilkin, N. S. Zhiltsov, D. D. Krivoruchko, A. V. Skrylev, A. N. Mokeev, P. Andrew, M. Kempenaars, G. Vayakis and M.J. Walsh, *Integration of Thomson scattering and laser-induced fluorescence in ITER divertor*, *Nucl. Fusion* **59** (2019) 086052

[9] H. Murmann, S. Götsch, H. Röhr, H. Salzmann, K. H. Steuer, *The Thomson scattering systems on the ASDEX Upgrade tokamak*, *Rev. Sci. Instrum.* **63** (1992) 4941

[10] A. Kallenbach, H.-S. Bosch, S. de Peña Hempel, R. Dux, M. Kaufmann, V. Mertens, J. Neuhauser, W. Suttrop, H. Zohm, *Possible divertor solutions for a fusion reactor. Part I. Physical aspects based on present day divertor operation*, *Fusion Eng. Des.* **36** (1997) 101

[11] S. Potzel, M. Wischmeier, M. Bernert, R. Dux, F. Reimold, A. Scarabosio, S. Brezinsek, M. Clever, A. Huber, A. Meigs, M. Stamp, the ASDEX Upgrade team, JET-EFDA Contributors, *Formation of the high density front in the inner far SOL at ASDEX Upgrade and JET*, *J. Nucl. Mat.* **463** (2015) 541

[12] R. Diaz, R. Courchinoux, J. Luce, C. Rouyer, J. L. Rullier, J.-Y. Natoli, L. Lamaignére, *Experimental evidence of temporal and spatial incoherencies of Q-switched Nd:YAG nanosecond laser pulses*, *Appl. Phys. B* **121** (2015) 439

[13] K. C. Behler, H. Eixenberger, B. Kurzan, A. Lohs, K. Lüddecke, M. Maraschek, R. Merkel, G. Raupp, G. Sellmair, B. Sieglin, W. Treutterer, ASDEX Upgrade Team, *Recent diagnostic developments at ASDEX Upgrade with the FPGA implemented Serial I/O System "SIO2" and "Pipe2" DAQ periphery*, *Fusion Eng. Des.* **159** (2020) 111873

[14] B. Kurzan, M. Jakobi, H. Murmann, and ASDEX Upgrade Team, *Signal processing of Thomson scattering data in a noisy environment in ASDEX Upgrade*, *Plasma Phys. Control. Fusion* **46** (2004) 299

[15] B. Kurzan, H. D. Murmann, *Edge and core Thomson scattering systems and their calibration on the ASDEX Upgrade tokamak*, *Rev. Sci. Instrum.* **82** (2011) 103501

[16] A. Kallenbach, A. Carlson, G. Pautasso, A. Peeters, U. Seidel, H.-P. Zehrfeld, ASDEX Upgrade Team, *Electric currents in the scrape-off layer in ASDEX Upgrade*, *J. Nucl. Mat.* **290-293** (2001) 639